JOC Article

3-Bromozinc Propenyl Esters: An Experimental and Theoretical Study of the Unique Stereocrossover Observed in Their Addition to Aromatic and Aliphatic Aldehydes

A. Bottoni,* M. Lombardo, G. P. Miscione, J. B. Pujol Algué, and C. Trombini*

Dipartimento di Chimica "G. Ciamician", Università di Bologna, via Selmi 2, I-40126 Bologna, Italy

andrea.bottoni@unibo.it; claudio.trombini@unibo.it

Received August 13, 2007

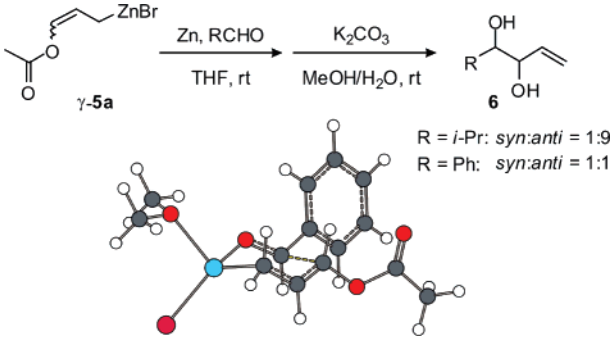

We report the results of a combined experimental and theoretical study on the reaction of 3-bromopropenyl acetate in the presence of zinc with three different aldehydes (i.e., benzaldehyde, 2-methylpropanal, and cyclohexanecarboxaldehyde). A 80% de in favor of the *anti* product has been experimentally observed with both saturated aldehydes, while for benzaldehyde, a 1:1 *syn*/*anti* ratio has been found. DFT computations show the existence of three η^1-allylic organozinc complexes [γ-(*Z*)-**5a**, γ-(*E*)-**5a**, and α-**5a**], very close in energy. Only γ-(*Z*)-**5a** and γ-(*E*)-**5a** lead to the observed product. The computational investigation of the reaction of these allylic organozinc complexes with benzaldehyde and 2-methylpropanal demonstrates in both cases the existence of two competitive reaction paths leading to the *syn* and *anti* adducts, respectively. An *anti* preference has been found for 2-methylpropanal with both γ-(*Z*)-**5a** and γ-(*E*)-**5a** species (a diastereoselectivity larger than 80% is predicted), in agreement with the experiment. With benzaldehyde, while the reaction of γ-(*Z*)-**5a** retains an *anti*-stereopreference (de = 70%), that involving γ-(*E*)-**5a** is characterized by two degenerate transition states. In this case, the agreement between computations and experiments would be satisfactory under the assumption that the initial oxidative addition affords the γ-(*E*)-**5a** zinc complex only. Additional MP2 computations have demonstrated that π-stacking interactions can play a significant role in determining the relative energy of the transition states leading to the *syn* and *anti* products.

Introduction

In the field of acyclic stereocontrol, the addition of allylic metal complexes **2** to carbonyl compounds **1** offers a powerful tool to the diastereo- and/or enantioselective (e.g., when L = chiral ligand) approach to synthons **3**, where a synthetically flexible carbon−carbon double bond is adjacent to two contiguous stereocenters (Scheme 1).[1] In the last three decades, most of the contributions in this field dealt with the study of crotyl complexes (A = Me)[1,2] and of oxygen-substituted allyl complexes (A = OR),[1b,3] while, as to the metal M, a wide range of choices is possible, from boron to indium, tin, and lead, getting across aluminum, silicon, and most of the metals of the fourth period.[4]

(1) For general reviews on this topic, see: (a) Chinchilla, R.; Nájera, C.; Yus, M. *Tetrahedron* **2005**, *61*, 3139−3176. (b) Denmark, S. E.; Fu, J. *Chem. Rev.* **2003**, *103*, 2763. (c) Katritzky, A. R.; Piffl, M.; Lang, H.; Anders, E. *Chem. Rev.* **1999**, *99*, 665−722. (d) Schlosser, M.; Desponds, O.; Lehmann, R.; Moret, E.; Rauchschwalbe, G. *Tetrahedron* **1993**, *49*, 10175−10203. (e) Hoffmann, R. W. *Angew. Chem., Int. Ed. Engl.* **1987**, *26*, 489−594. (f) Hoffmann, R. W. *Angew. Chem., Int. Ed. Engl.* **1982**, *21*, 555−642.

(2) Roush, W. R. In *Comprehensive Organic Synthesis*; Trost, B. M, Heathcock, C. H., Eds.; Pergamon Press: Oxford, 1991; Vol. II, pp 1−53.

(3) (a) Lombardo, M.; Trombini, C. *Chem. Rev.* **2007**, *107*, 3843−3879. (b) Marshall, J. A. *Chem. Rev.* **1996**, *96*, 31−47.

10.1021/jo701661z CCC: $40.75
Published on Web 12/22/2007

SCHEME 1

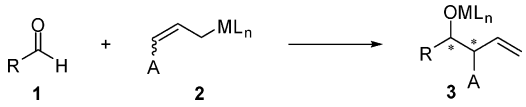

High levels of simple diastereoselectivity in the reaction of **2** with prochiral aldehydes are often achieved; in these cases, preferential formation of *syn* or *anti* adducts **3** can be anticipated on the basis of two general trends. Allylic boranes and boronates are representative of allylic organometallics which afford *syn* or *anti* adducts as a function of the carbon−carbon double bond configuration. Chair-like Zimmermann−Traxler transition states (TS) offer a rationale to the diastereoselective formation of *syn* adducts **3** starting from (*Z*)-**2**, while the *E*-configured ones afford *anti*-**2**. A second family of complexes **2**, typically stannanes[3] and chromium complexes,[5] stereoconverge either to *syn* or *anti* products, independently of the C=C bond configuration, the stereopreference being dictated by the metal only. The stereoconvergence is rationalized in terms of the open-chain TS in the case of stannanes and in terms of a rapid fluxional equilibration between (*Z*)-**2** and (*E*)-**2** in the case of chromium complexes. The latter species produce *anti* adducts via cyclic TS involving the kinetically more reactive (*E*)-**2** complexes.

We recently proposed to the attention of synthetic chemists a new family of ester-substituted allyl organometallics **5**, derived from the insertion of Zn(0), In(0), and Cr(II) into the carbon−halogen bond of 3-halopropenyl esters **4** (Scheme 2).[6] The versatility of **5** was confirmed both by Petrini and co-workers,[7] who exploited **5** (M = Zn) in a synthesis of *anti*-4-aminoalk-1-en-3-ols, and by Palmelund and Madsen, who used **5** (M = In) as a two-carbon homologating agent for the preparation of higher sugars.[8]

SCHEME 2

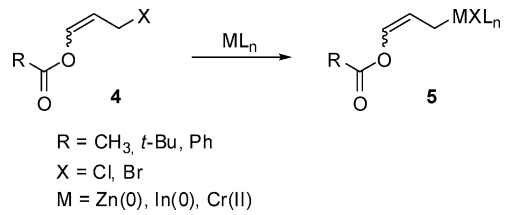

Complexes **5** (M = Zn and In; R = CH_3), as well as the corresponding carbonates (R = MeO) more recently developed in our lab,[9] display a unique behavior when reacted with simple prochiral aldehydes: they preferentially afford *syn* adducts with conjugated and aromatic aldehydes, and an *anti* adduct when they add to saturated aldehydes. Here a combined experimental−theoretical approach aimed at shedding light on factors controlling the stereochemical outcome of the addition of **5** to prochiral aldehydes is presented.

TABLE 1. Zinc-Mediated Grignard Route to Alk-1-en-3,4-diols 6[a]

entry	RCHO	**6** yield[b] (%)	*syn*-**6**/*anti*-**6**
1	**1a** (R = Ph)	70	50:50
2	**1b** (R = *i*-Pr)	71	10:90
3	**1c** (R = *c*-C_6H_{11})	72	10:90

[a] The following molar ratios were used: zinc/**4a**/aldehyde = 2:1.5:1. [b] Isolated yields after flash chromatography on SiO_2.

Results and Discussion

Experimental Studies. To meet theoretical feasibility and accuracy requirements, we selected among various esters **4**, 3-bromopropenyl acetate **4a** (R = CH_3, X = Br) as substrate for our model reaction, and zinc as the metal. The experimental plan involved the investigation of the reaction of **4a** with zinc in the presence of three model aldehydes representative of conjugated and saturated aldehydes, namely, benzaldehyde (**1a**, R = Ph) on one hand and 2-methylpropanal (**1b**, R = *i*-Pr) and cyclohexanecarboxaldehyde (**1c**, R = *c*-C_6H_{11}) on the other. Compound **4a** was used as a 65:35 *Z*/*E* isomer mixture, as obtained by distillation after the addition of acetyl bromide to acrolein.[10] For the model reaction, the solvent used was THF (replaced by dimethylether in silico), and the reactions were run according to a two-step Grignard protocol involving formation of the organometallic species followed by the addition of the aldehyde. To determine the diastereomeric composition, the reaction mixtures were hydrolyzed with K_2CO_3 in 4:1 MeOH/H_2O in order to free the known alk-1-en-3,4-diols **6** (Scheme 3).

SCHEME 3[a]

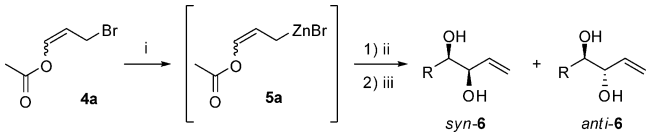

[a] Reagents and conditions: (i) Zn, THF, 0 °C → 20 °C, 2 h; (ii) RCHO, 20 °C, 2 h; (iii) KB_2CO_3 (3 equiv), CH_3OH/H_2O (4:1 v/v), 20 °C, 2 h.

The results obtained in this set of reactions are collected in Table 1. Under these conditions, 80% de values were obtained with both saturated aldehydes in favor of *anti*-**6** (Table 1, entries 2 and 3), meaning that the energy difference $\Delta\Delta E^{\ddagger}$ between the two diastereomorphic TS is in the range of ∼0.5 kcal mol^{-1}. On the other hand, perfectly degenerate diastereomorphic TS are involved in the reaction of **4a** with benzaldehyde, given that a 1:1 *syn*/*anti* ratio was observed (Table 1, run 1).

It is worthy to note the minor but not negligible role played by the metal/solvent pair in stereoselectivity, particularly, in determining the *syn*/*anti* ratio with the aromatic aldehyde.

(4) Yamamoto, Y.; Asao, N. *Chem. Rev.* **1993**, *93*, 2207−2293.
(5) Fürstner, A.; Shi, N. *J. Am. Chem. Soc.* **1996**, *118*, 12349−12357.
(6) (a) Lombardo, M.; Girotti, R.; Morganti, S.; Trombini, C. *Org. Lett.* **2001**, *3*, 2981−2983. (b) Lombardo, M.; Girotti, R.; Morganti, S.; Trombini, C. *Chem. Commun.* **2001**, 2310−2311. (c) Lombardo, M.; Licciulli, S.; Morganti, S.; Trombini, C. *Synlett* **2003**, 43−46. (d) Lombardo, M.; Morganti, S.; Trombini, C. *J. Org. Chem.* **2003**, *68*, 997−1006. (e) Lombardo, M.; d'Ambrosio, F.; Morganti, S.; Trombini, C. *Tetrahedron Lett.* **2003**, *44*, 2823−2826. (f) Lombardo, M.; Licciulli, S.; Morganti, S.; Trombini, C. *Chem. Commun.* **2003**, 1762−1763. (g) Lombardo, M.; Licciulli, S.; Trombini, C. *Pure Appl. Chem*. **2004**, *76*, 657−669. (h) Lombardo, M.; Gianotti, K.; Licciulli, S.; Trombini, C. *Tetrahedron* **2004**, *60*, 11725−11732. (i) Lombardo, M.; Licciulli, S.; Rispoli, G.; Trombini, C.; Dhavale, D. D. *Tetrahedron Lett.* **2005**, *46*, 3789−3792.
(7) (a) Petrini, M.; Profeta, R.; Righi, P. *J. Org. Chem*. **2002**, *67*, 4530. (b) Giri, N.; Petrini, M.; Profeta, R. *J. Org. Chem.* **2004**, *69*, 7303.
(8) (a) Palmelund, A.; Madsen, R. *J. Org. Chem*. **2005**, *70*, 8248−8251. (b) Keinicke, L.; Fristrup, P.; Norrby, P.-O.; Madsen, R. *J. Am. Chem. Soc.* **2005**, *127*, 15756−15761.
(9) (a) Lombardo, M.; Pasi, F.; Tiberi, C.; Trombini, C. *Synthesis (Special Topic*) **2005**, 2609−2614. (b) Lombardo, M.; Pasi, F.; Trombini, C. *Eur. J. Org. Chem.* **2006**, 3061. (c) Lombardo, M.; Capdevila, M. G.; Pasi, F.; Trombini, C. *Org. Lett*. **2006**, *8*, 3303.
(10) (a) Ulich, L. H.; Adams, R. *J. Am. Chem. Soc*. **1921**, *45*, 660−667. (b) Neuenschwander, M.; Bigler, P.; Christen, K.; Iseli, R.; Kyburz, R.; Mühle, H. *Helv. Chim. Acta* **1978**, *61*, 2047−2058.

Indeed, in previous works, this ratio was 70:30 using both Zn in aq NH_4Cl[6a] and indium in THF at 20 °C, while it increased to 85:15 using indium in THF at −50 °C.[6b]

In any case, also using the system Zn/THF, the presence of an unidentified effect counteracting the *anti* diastereopreference exhibited with saturated aldehydes was apparent using benzaldehyde. Using cyclohexanecarboxaldehyde, the *syn*/*anti* ratio was almost the same in three different reaction conditions, where it ranged from 15:85 (In/THF) to 10:90 (Zn/aq NH_4Cl and Zn/THF).

A second set of experiments (Table 2) was also carried out in order to possibly evaluate the role of the ester moiety on the reaction stereoselectivity. To this purpose, we prepared (*E*)-3-bromopropenyl benzoate **4b** (R = Ph), a sample of **4b** as a *Z*/*E* = 55:45 mixture, and 3-chloropropenyl pivalate **4c** (R = *t*-Bu; *Z*/*E* = 75:25). The stereochemical outcomes of zinc-promoted reactions of (*E*)-**4b** and of the *E*/*Z* isomeric mixture of **4b** with benzaldehyde (Table 2, entries 1 and 2) and cyclohexanecarboxaldehyde (Table 2, entries 3 and 4) were virtually identical, meaning that the stereochemical composition of starting halide does not affect the stereochemical nature of the intermediate zinc complexes **5**. With respect to chloride **4c**, which is much less reactive toward zinc insertion into the C−Cl bond, the adoption of a one-pot Barbier protocol is more effective than the previously adopted two-step Grignard procedure (Table 2, entries 5−7). Moreover, the final deprotection step is carried out with $LiAlH_4$ to completely remove the pivalate ester (Scheme 4).

TABLE 2. Reactions of 3-Bromopropenyl Benzoate 4b and of 3-Chloropropenyl Pivalate 4c[a]

run	4	RCHO	t[b] (h)	6 yield[c] (%)	*syn*-6/*anti*-6
1	(*E*)-**4b**	**1a**	2	80	55:45
2	(*E*/*Z*)-**4b**	**1a**	2	85	50:50
3	(*E*)-**4b**	**1c**	2	80	15:85
4	(*E*/*Z*)-**4b**	**1c**	2	80	15:85
5	**4c**	**1a**	24	65	40:60
6	**4c**	**1b**	24	40	>5:95
7	**4c**	**1c**	24	55	10:90

[a] The following molar ratios were used: zinc/**4b** or **4c**/aldehyde = 2:1.5:1. [b] Reaction time after the addition of the aldehyde. [c] Isolated yields after flash chromatography on SiO_2.

SCHEME 4[a]

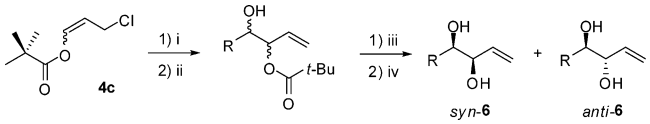

[a] Reagents and conditions: (i) Zn, RCHO, THF, 20 °C, 24 h; (ii) aq NH_4Cl; (iii) $LiAlH_4$, THF, 0 °C, 2 h; (iv) aq NH_4Cl.

It is worthy to note the substantial lack of effect on the stereoselectivity of the three addition reactions exerted by the conjugation of the C=O group with the phenyl ring in **4b**, which almost afford the same results of acetate **4a**. Regarding the much more sterically congested pivalate **4c**, reactions considerably slow down as expected, but *anti* stereoselectivity slightly improves in all cases. Again, the 40:60 *syn*/*anti* ratio recorded with benzaldehyde clearly suggests the presence of an unidentified effect, which opposes the more favored reaction channel, which leads to the formation of an *anti* adduct.

Computational Methods. All DFT and MP2 computations reported here have been carried out with the Gaussian 03[11] series of programs. The nonlocal hybrid Becke's three-parameter exchange functional (denoted as B3LYP in the Gaussian formalism) has been used for DFT computations. At both DFT and MP2 levels, we have employed the DZVP basis, which is a local spin density (LSD) optimized basis set of double-ζ quality.[12] This basis, which includes polarization functions, is suitable to describe metal−ligand interactions such as those occurring in the systems investigated here. The locally dense basis set (LDBS)[13] approach has been chosen for DFT computations involving benzaldehyde. In this case, the CHO functional group and the α ring carbon have been described at the DZVP level, while the less accurate 3-21G* basis has been used for the remaining atoms of the benzene ring. The geometry of the various critical points on the reaction surface has been fully optimized with the gradient method available in Gaussian 03. A computation of the harmonic vibrational frequencies has been carried out to determine the nature of each critical point and to obtain ZPE (zero point energy) corrections and Gibbs energy values at room temperature.

Theoretical Studies. We have first examined the structure and the fluxional interconversion reactions of the organometallic reagents derived from the insertion of a zinc atom into the carbon−halogen bond of 3-bromopropenyl acetate **4a**, in the presence of two molecules of dimethylether, which represent the coordinating solvent. Three different *σ*-bonded (η^1) complexes (**5a**) exist. These are the two stereoisomers, γ-(*E*)-**5a** and γ-(*Z*)-**5a**, and the structural isomer α-**5a**. The reversible metallotropic shifts responsible for the interconversion between γ-(*E*)-**5a** and γ-(*Z*)-**5a** are outlined in Scheme 5. The investigation of the potential surface has shown that this fluxional equilibrium involves two transition states, **TS-1** and **TS-2** (see Figure 1) connecting the three η^1 complexes.

SCHEME 5

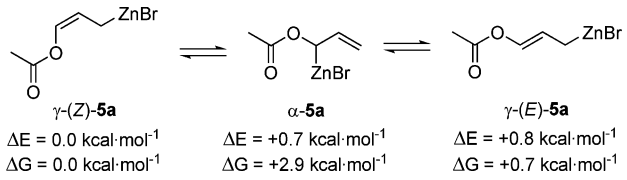

These three η^1 species are very close in energy, with γ-(*Z*)-**5a** being the most stable isomer. Furthermore, γ-(*Z*)-**5a** and γ-(*E*)-**5a** have similar geometric parameters. In both cases, the

(11) Frisch, M. J.; Trucks, G. W.; Schlegel, H. B.; Scuseria, E. G.; Robb, M. A.; Cheeseman, J. R.; Zakrzewski, V. G.; Montgomery, J. A., Jr.; Stratmann, R. E.; Burant, J. C.; Dapprich, S.; Millam, J. M.; Daniels, A. D.; Kudin, K. N.; Strain, M. C.; Farkas, O.; Tomasi, J.; Barone, V.; Cossi, M.; Cammi, R.; Mennucci, B.; Pomelli, C.; Adamo, C.; Clifford, S.; Ochterski, J.; Petersson, G. A.; Cui, Q.; Morokuma, K.; Malik, D. K.; Rabuck, A. D.; Raghavachari, K.; Foresman, J. B.; Cioslowski, J.; Ortiz, J. V.; Stefanov, B. B.; Liu, G.; Liashenko, A.; Piskorz, P.; Kamaromi, I.; Gomperts, R.; Martin, R. L.; Fox, D. J.; Keith, T.; Al-Laham, M. A.; Peng, C. Y.; Nanayakkara, A.; Gonzalez, C.; Challacombe, M.; Gill, P. M. W.; Johnson, B. G.; Chen, W.; Wong, M. W.; Andres, J. L.; Gonzalez, C.; Head-Gordon, M.; Replogle, E. S.; Pople, J. A. *Gaussian 98*, revision A.6; Gaussian, Inc.: Pittsburgh, PA, 1998.

(12) (a) Godbout, N.; Salahub, D. R.; Andzelm, J.; Wimmer, E. *Can. J. Chem.* **1992**, *70*, 560−571. (b) *UniChem DGauss*, version 2.3.1; Cray Research, Inc., 1994.

(13) (a) Di Labio, G. A.; Pratt, D. A.; Wright, J. S. *Chem. Phys. Lett.* **1998**, *297*, 181−186. (b) Wright, J. S.; Johnson, E. R.; Di Labio, G. A. *J. Am. Chem. Soc.* **2001**, *123*, 1173−1183.

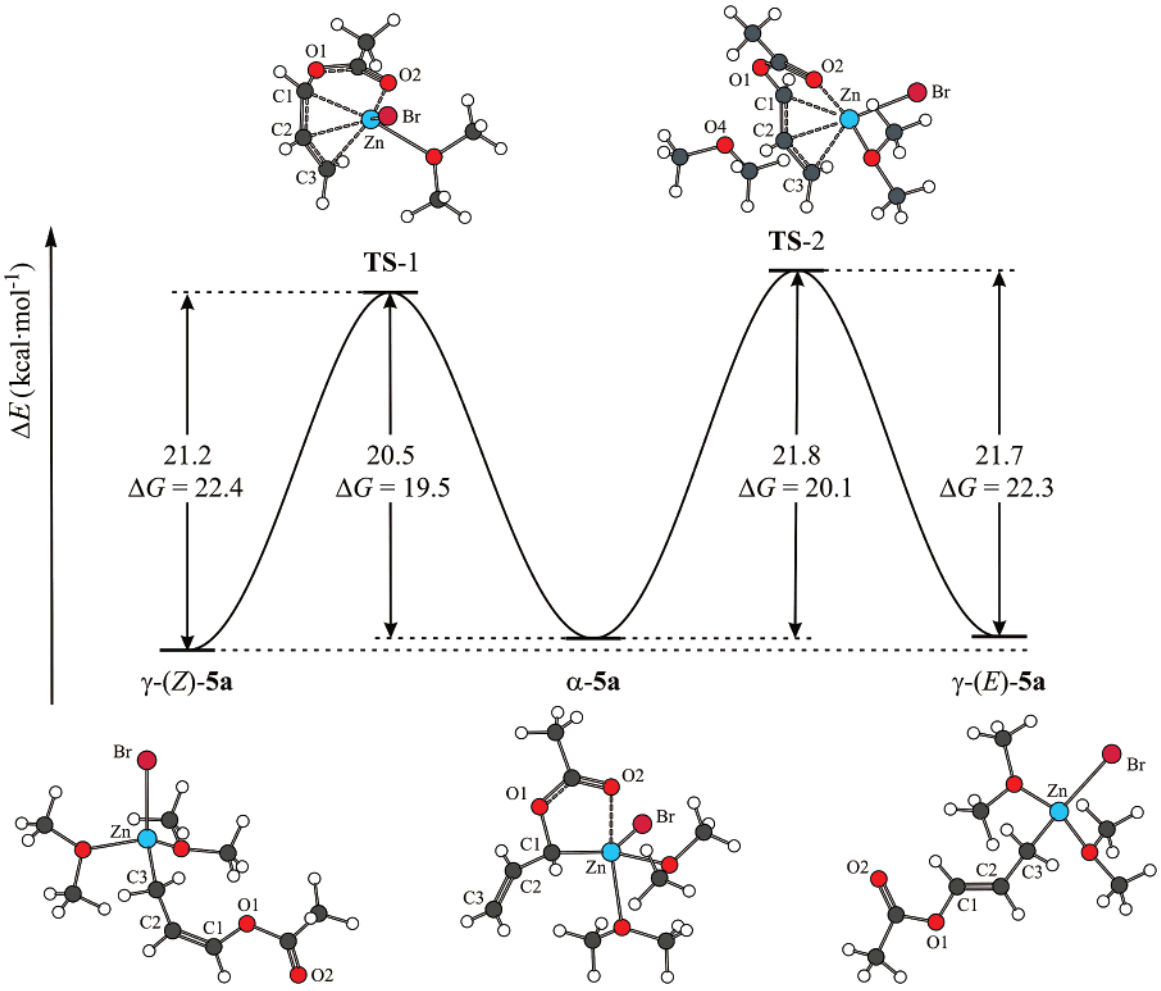

FIGURE 1. Energy profile for the fluxional equilibrium of γ-(*Z*)-**5**, α-**5a**, and γ-(*E*)-**5a**.

TABLE 3. Selected Bond Lengths (Å) for γ-(*Z*)-5a, TS-1, α-5a, TS-2, and γ-(*E*)-5a

	Zn−Br	Zn−O2	Zn−C1	Zn−C2	Zn−C3	C1−C2	C2−C3
γ-(*Z*)-**5a**	2.388	6.244	3.920	2.980	2.016	1.342	1.486
TS-1	2.363	2.096	2.324	2.250	2.473	1.422	1.391
α-**5a**	2.392	2.433	2.054	3.046	4.014	1.485	1.343
TS-2	2.356	2.239	2.317	2.194	2.352	1.406	1.411
γ-(*E*)-**5a**	2.390	5.927	3.910	2.975	2.014	1.339	1.489

zinc atom is bonded to bromine, two dimethylether molecules, and the acetoxyallyl ligand in a typical tetrahedral arrangement (see Table 3).

The structure of the α-**5a** isomer is remarkably different. The zinc atom is penta-coordinated with the acetoxyallyl fragment acting as a bidentate ligand and forming a five-membered ring where the Zn−O2 and Zn−C1 distances are 2.433 and 2.054 Å, respectively. The metal atom has a trigonal bipyramidal configuration with the carbonyl oxygen (O2) and one dimethylether molecule in axial positions. The new Zn−O2 interaction is responsible for a slight weakening of the remaining four metal−ligand bonds. This effect is particularly evident for the bond with the axial dimethylether molecule (Zn−O = 2.393 Å), as a result of the carbonyl oxygen *trans* influence.

The transformation γ-(*Z*)-**5a** → α-**5a** involves the transition state **TS-1** (left side of Figure 1) and has a barrier of 21.2 kcal mol^{-1}. This suggests a very slow equilibration at room temperature. **TS-1** has basically an η^3 structure, where a strong weakening of the Zn−C3 and C1−C2 π bonds and the simultaneous formation of the Zn−C1 and C2−C3 π bonds are evident. Essentially, the metal "slides" along the three carbon atoms of the allyl unit. Moreover, since the transition state involves only one dimethylether molecule, to obtain the α-**5a** isomer, a second solvent molecule must enter the metal coordination sphere, causing the simultaneous breaking of the Zn−(C1−C2) π-bond interaction. Our computations show that this final step involving the insertion of the second dimethylether molecule does not require any activation barrier.

The path for the γ-(*E*)-**5a** → α-**5a** transformation (Figure 1, right side) is similar to the previous one, with a slightly larger barrier (21.7 kcal mol^{-1}). The corresponding transition state **TS-2** is again characterized by an η^3 structure. Compared to **TS-1**, the zinc−carbon interactions are stronger (the Zn−C1, Zn−C2, and Zn−C3 distances become 2.317, 2.194, and 2.352 Å, respectively), while those involving zinc and oxygen are weaker (the Zn−O2 distance varies from 2.096 in **TS-1** to 2.239 Å in **TS-2**) as a result of a higher angular strain. The breaking of the Zn−(C1−C2) π-bond interaction and the simultaneous formation of a new Zn−dimethylether bond are required to form the α-**5a** isomer. As previously observed, the insertion of an additional solvent molecule occurs without any barrier, as confirmed by IRC calculations. Actually, in **TS-2**, the second dimethylether molecule is idling far away from the zinc atom,

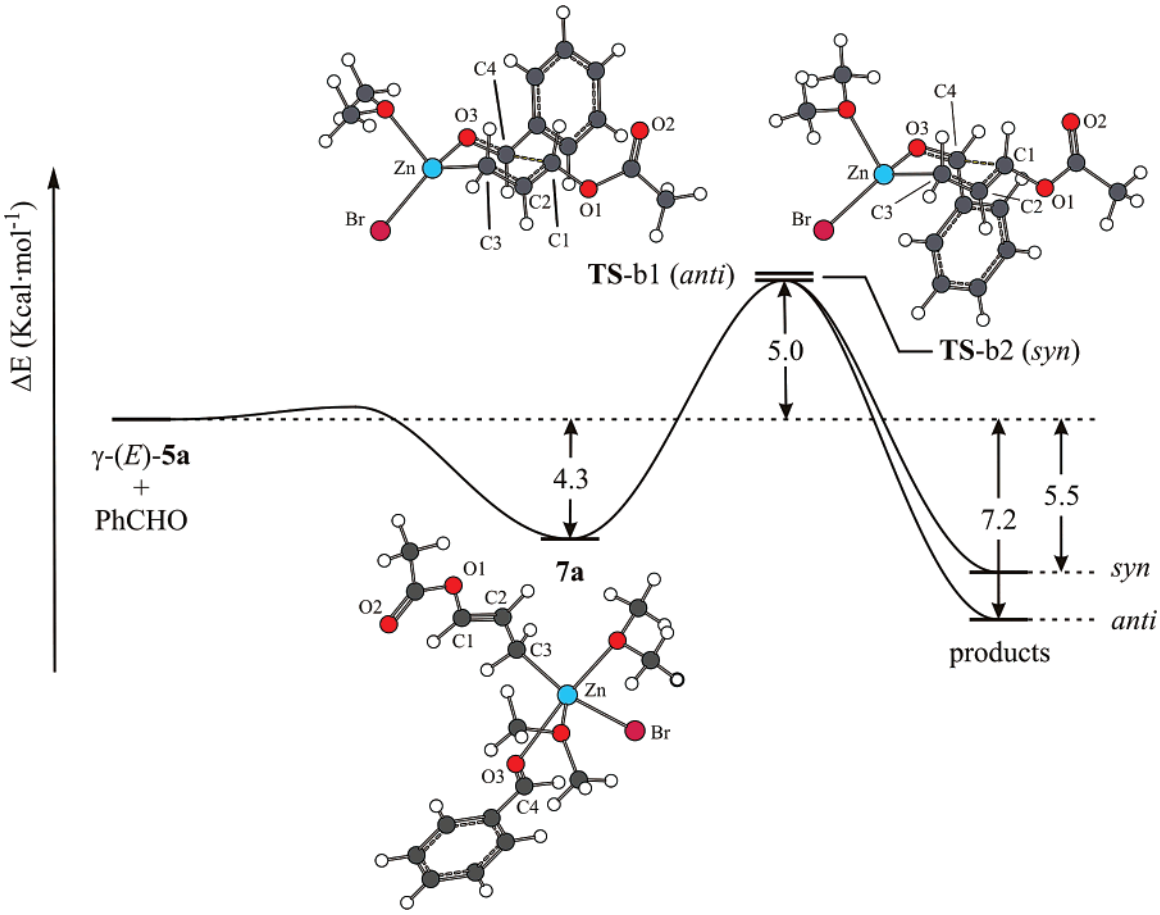

FIGURE 2. Energy profile for the addition of γ-(*E*)-**5a** to benzaldehyde (**1b**) obtained at the DFT level.

with the Zn−O4 distance being 4.560 Å. At this distance, no significant interactions can be detected.

When we consider the Gibbs free energy values, the α-**5a** → γ-(*E*)-**5a** transformation remains slightly favored over the conversion of α-**5a** into γ-(*Z*)-**5a** (the two barriers are almost identical: 19.5 and 20.1 kcal mol^{-1}). However, the relative thermodynamic stability of the three isomers changes: γ-(*Z*)-**5a** is still the most stable, but the stabilities of γ-(*E*)-**5a** (0.7 kcal mol^{-1}) and α-**5a** (2.9 kcal mol^{-1}) are reversed. This is probably due to the loss of entropy in the α-**5a** species when the additional Zn−dimethylether bond forms. Irrespective of the energy barriers, clearly indicating that fluxionality is a slow process at room temperature, if a perfect thermodynamic equilibration were attained, the Gibbs free energy values reported would predict the following isomer ratio: γ-(*Z*)-**5a**/γ-(*E*)-**5a**/α-**5a** ∼ 75:24:1.

Summarizing the results discussed so far, no difference in chemical yields and diastereomeric composition was observed using different geometric composition of benzoate **4b** with the three model aldehydes chosen (see previous section). On the other hand, calculations disclosed that γ-(*Z*)-**5a** and γ-(*E*)-**5a** should be configurationally stable at 0−20 °C on thermodynamic grounds. A preliminary conclusion is that the unknown mixture of γ-(*Z*)-**5** and γ-(*E*)-**5** present in solution for each substrate examined is the result of the unknown oxidative addition process and does depend either on the isomeric composition of the starting 3-halopropenyl esters **4** or on fluxional equilibration taking place after the oxidative addition step. As a consequence, to find a rationale accounting for the experimental behavior of 3-halopropenyl esters **4**, we have modeled and compared all the possible nucleophilic addition paths of γ-(*Z*)-**5** and γ-(*E*)-**5** to aromatic and aliphatic aldehydes.

We have also investigated the potential surface for the reactions of aldehydes with α-**5a**, even though the corresponding 4-hydroxyenol acetate derivatives have never been experimentally detected. These results are reported for completion in the Supporting Information.

TABLE 4. Selected Bond Lengths (Å) for 7a, TS-b1, and TS-b2

	Zn−Br	Zn−O3	Zn−C3	C1−C2	C2−C3	C1−C4
7a	2.428	2.574	2.021	1.340	1.488	5.956
TS-b1	2.367	1.979	2.139	1.397	1.412	2.148
TS-b2	2.369	1.966	2.151	1.399	1.406	2.152

Addition of Zinc Complexes γ-(*E*)-5a and γ-(*Z*)-5a to Benzaldehyde (1b). In this section, we discuss the addition of zinc−bromopropenyl acetate complexes γ-(*E*)-**5a** and γ-(*Z*)-**5a** to benzaldehyde (**1a**).

Addition of γ-(*E*)-5a Complex. The energy profile for the addition of γ-(*E*)-**5a** to benzaldehyde is shown in Figure 2, and selected bond lengths for the intermediate **7a** and the two transition states **TS-b1** and **TS-b2** are reported in Table 4. A barrier-free preassociation of the aldehyde with the metal leads to the formation of the penta-coordinated intermediate **7a**, which is 4.3 kcal mol^{-1} more stable than reactants [γ-(*E*)-**5a** + PhCHO]. As a matter of fact, the region of the potential surface corresponding to the formation of **7a** is extremely flat, and in spite of extensive search, no transition states were located. It has been observed that zinc can rather easily change its

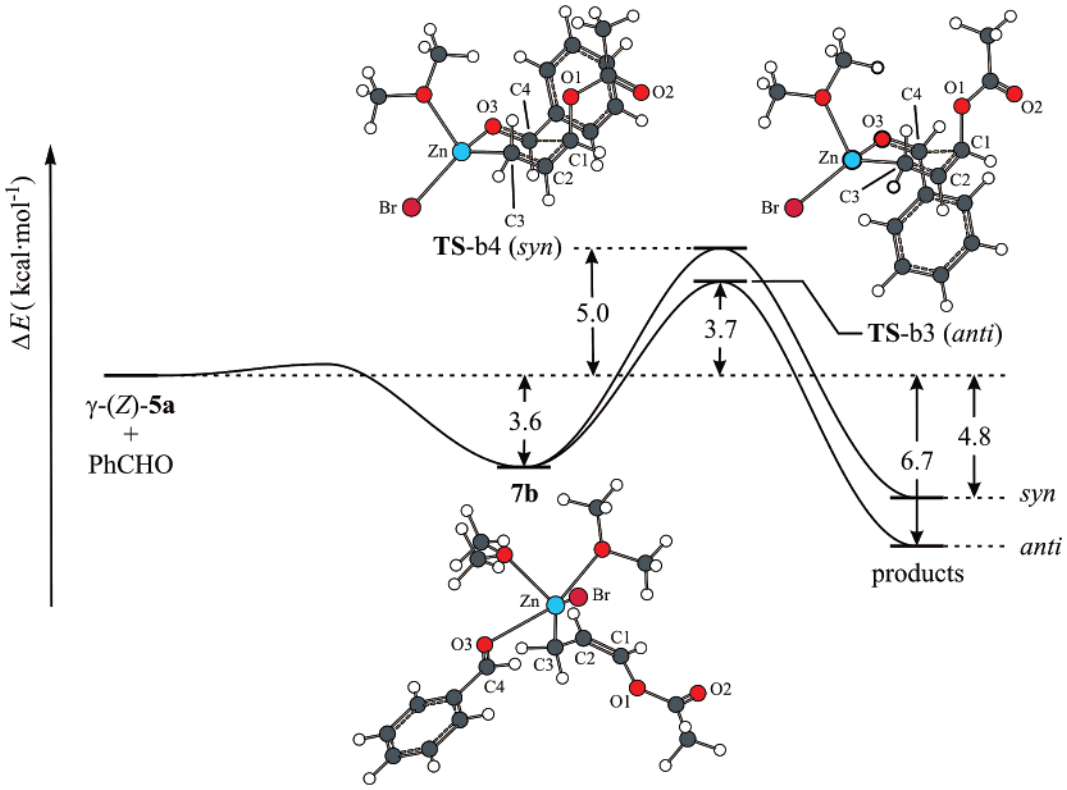

FIGURE 3. Energy profile for the addition of γ-(*Z*)-**5a** to benzaldehyde (**1b**) obtained at the DFT level.

coordination state (four/five) by accepting and releasing a ligand. In particular, in the present case, because of the small steric hindrance around the metal in the tetrahedral configuration, the approach and binding of an additional (fifth) ligand can occur rather easily with a negligible geometric distortion and, consequently, without significant energy barrier. In the trigonal bipyramidal structure of **7a**, the aldehyde and a dimethylether molecule are axial, whereas the second dimethylether molecule, the bromine atom, and the carbon chain occupy the equatorial positions. The axial zinc−dimethylether bond (2.482 Å) is longer than the corresponding equatorial one (2.234 Å), as a consequence of the *trans* effect of the aldehyde. In general, all the zinc−ligand interactions in **7a** are slightly weaker when compared to the starting tetra-coordinated complex γ-(*E*)-**5a**, which makes easier the expulsion of a ligand from the metal coordination sphere.

Two different channels for the addition reaction originate from **7a**, depending on the heterotopic faces of the aldehyde and intermediate **7a**. The *re*−*re* (or *si*−*si*) approach leads to the *syn* product, while the *re*−*si* (or *si*−*re*) approach affords the *anti* product. The two transition states, **TS-b1** and **TS-b2**, leading to the *anti* and *syn* isomers, respectively, are placed at the same energy, and thus, the corresponding intrinsic barriers are identical [9.3 kcal mol^{-1}, corresponding to the sum of the absolute values of the relative energy of the intermediate (4.3 kcal mol^{-1}) and transition states (5.0 kcal mol^{-1}) with respect to reactants]. If the Gibbs free energy (ΔG) is considered, a slight preference for **TS-b1**, affording the *anti* product, ensues (the difference in the Gibbs free energy $\Delta\Delta G$ is 0.2 kcal mol^{-1}). Thus, in this case, the identical (or almost identical) energy of the two transition states is in agreement with the 1:1 *syn*/*anti* ratio experimentally observed.

Both **TS-b1** and **TS-b2** are six-membered cyclic structures in a chair conformation, where the acetate group and the dimethylether molecule are equatorial. On the contrary, the aromatic ring is equatorial in **TS-b1** and axial in **TS-b2**. Therefore, the main difference between the two transition states is represented by the different relative position of the phenyl and acetate groups, which are closer in **TS-b1** where they face each other at a distance of about 3.20 Å. In the two transition states, the advancement of the reaction is revealed by the strengthening of the Zn−O3 bond with respect to **7a**. Also, the almost identical C2−C3 and C1−C2 bond lengths (∼1.4 Å) in **TS-b1** and **TS-b2** indicate that the transition state is approximately halfway between reactants and products along the reaction coordinate.

TABLE 5. Selected Bond Lengths (Å) for 7b, TS-b3, and TS-b4

	Zn−Br	Zn−O3	Zn−C3	C1−C2	C2−C3	C1−C4
7b	2.421	2.692	2.020	1.342	1.483	6.406
TS-b3	2.371	1.982	2.158	1.392	1.408	2.154
TS-b4	2.365	1.984	2.158	1.395	1.405	2.175

Addition of γ-(*Z*)-5a Complex. The energy profile for the reaction of γ-(*Z*)-**5a** with benzaldehyde (Figure 3 and Table 5) is similar to that found for γ-(*E*)-**5a**. Again, an initial penta-coordinated intermediate (**7b**, 3.6 kcal mol^{-1} more stable than reactants) is observed. The removal of a dimethylether molecule and the formation of the new carbon−carbon bond simultaneously occur in the subsequent step along two different channels leading to the *anti* and *syn* products, respectively.

As a matter of fact, two transition states connecting **7b** to the *anti* product have been located. The more stable one (**TS-b3**, reported in Figure 3) has again a six-membered chair-like structure and corresponds to an intrinsic energy barrier of 7.3 kcal mol^{-1}. The three bulkiest substituents (i.e., the aromatic ring, the dimethylether, and the acetate group) are placed in such a way to reduce the steric repulsion (the

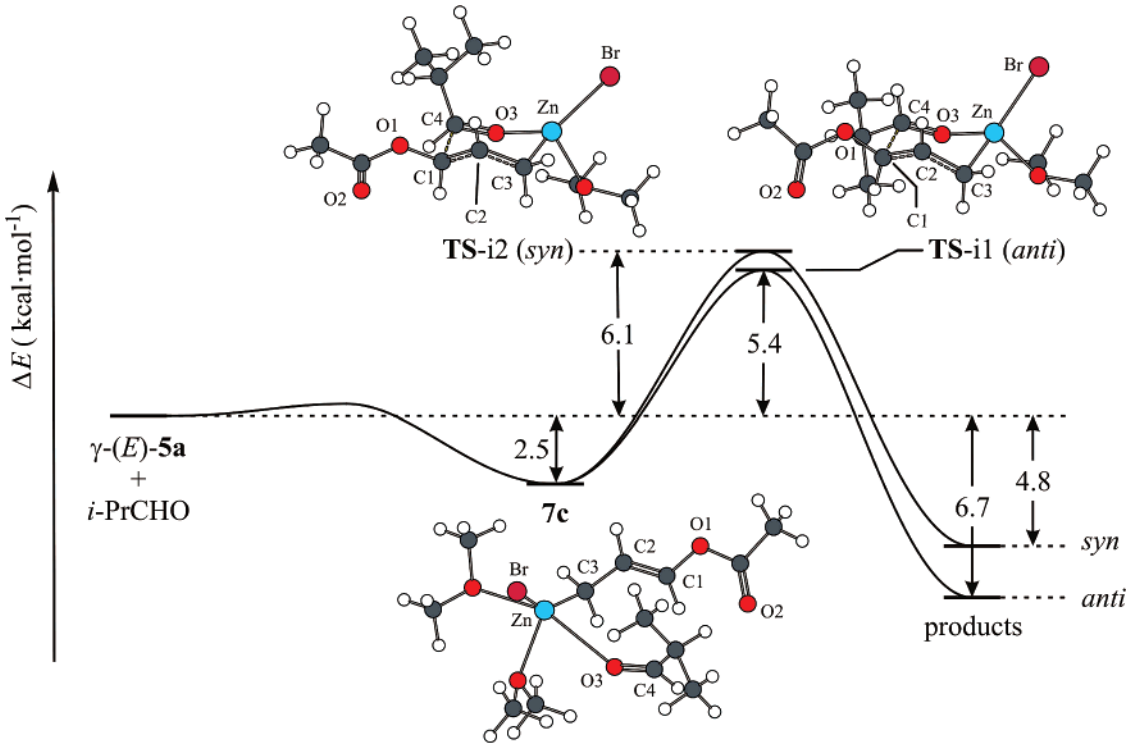

FIGURE 4. Energy profile for the addition of γ-(*E*)-**5a** to 2-methylpropanal (**1b**) obtained at the DFT level.

TABLE 6. Selected Bond Lengths (Å) for 7c, TS-i1, and TS-i2

	Zn−Br	Zn−O3	Zn−C3	C1−C2	C2−C3	C1−C4
7c	2.395	2.785	2.017	1.339	1.488	3.530
TS-i1	2.369	1.998	2.117	1.388	1.420	2.205
TS-i2	2.368	1.987	2.125	1.390	1.417	2.180

dimethylether molecule is equatorial, while the benzene ring and the acetate are *trans* and axially oriented). The dihedral angle C1−C4−O3−Zn is −48.7°. The second transition structure, which can lead to the *anti* adduct (Figure S12 in the Supporting Information) is 5.9 kcal mol^{-1} higher than that of **TS-b3**. Here, the zinc atom coordinates the carbonyl oxygen of the acetate fragment adopting a boat-like conformation. In this case, the interaction of the metal with a fifth ligand is not able to balance the strain associated with the bicyclic structure.

A chair-like six-membered structure characterizes also the transition state affording the *syn* adduct (**TS-b4**). The corresponding energy barrier is 8.6 kcal mol^{-1}. It is interesting to outline that, similarly to **TS-b1**, the phenyl and acetate systems are face-to-face oriented, and therefore, an attractive π-stacking interaction is conceivable. However, this type of interaction, which could be effective also at large distances (about 3.0 Å in the present case), is not properly described by the DFT method, and hence destabilizing steric effects prevail.

Thus, a more significant energy difference (1.3 kcal mol^{-1}) between the two transition states (**TS-b3** for *anti* and **TS-b4** for *syn*) characterizes the present case with respect to that involving the γ-(*E*)-**5a** isomer, and the preference for the path leading to the *anti* isomer becomes more evident. When we take into account the entropy contribution, the corresponding free energy difference between the two transition states ($\Delta\Delta G^{\ddagger}$) becomes 1.0 kcal mol^{-1}. This value would afford a diastereoselectivity of about 70%, in contrast to the experimental evidence.

The structures of **TS-b1** (Figure 2) and **TS-b4** (Figure 3), leading to the *syn* and *anti* adducts, respectively, deserve a further analysis. As previously outlined, in both cases, the phenyl ring and the acetate group are placed on almost parallel planes, a geometric requirement to activate stabilizing π-stacking interactions. To provide a reliable description of these interactions and obtain more accurate relative energy values, we have carried out MP2 computations with full geometry optimization on **TS-b1**, **TS-b2**, **TS-b3**, and **TS-b4** and the intermediates **7a** and **7b**. A schematic representation of the MP2 structures is given in the Supporting Information. The MP2 results confirm the importance of π-stacking effects. At the MP2 level, **TS-b1** and **TS-b2** remain very close in energy (the corresponding energy barriers are 10.9 and 11.3 kcal mol^{-1}, respectively). More important, the energy gap between **TS-b4** and **TS-b3** decreases (from 1.3 to 0.5 kcal mol^{-1}), although the relative stability is reversed; that is, the *syn* path becomes more favored (the corresponding intrinsic energy barriers become 9.1 and 8.6 kcal mol^{-1} for *syn* and *anti*, respectively). Thus, these results suggest that π-stacking interactions have the effect of making **TS-b4** and **TS-b3** closer in energy, and consequently, the diastereoselectivity in favor of the *anti* product (as obtained at the DFT level) should decrease, in agreement with the experimental observation.

Since the difference between the compared barriers is sometimes less than 1.0 kcal mol^{-1}, an additional important point concerning the reliability of these values should be outlined. Even if the absolute value of barrier heights is certainly characterized by an error larger than 1.0 kcal mol^{-1}, it is conceivable that, since the transition states are diastereomers, we can trust a considerable cancellation of error when we consider barrier height differences.

Addition of Zinc Complexes γ-(*E*)-5a and γ-(*Z*)-5a to 2-Methylpropanal (1b). In this section, we examine in detail the singlet potential energy surface for the addition of γ-(*E*)-**5a**

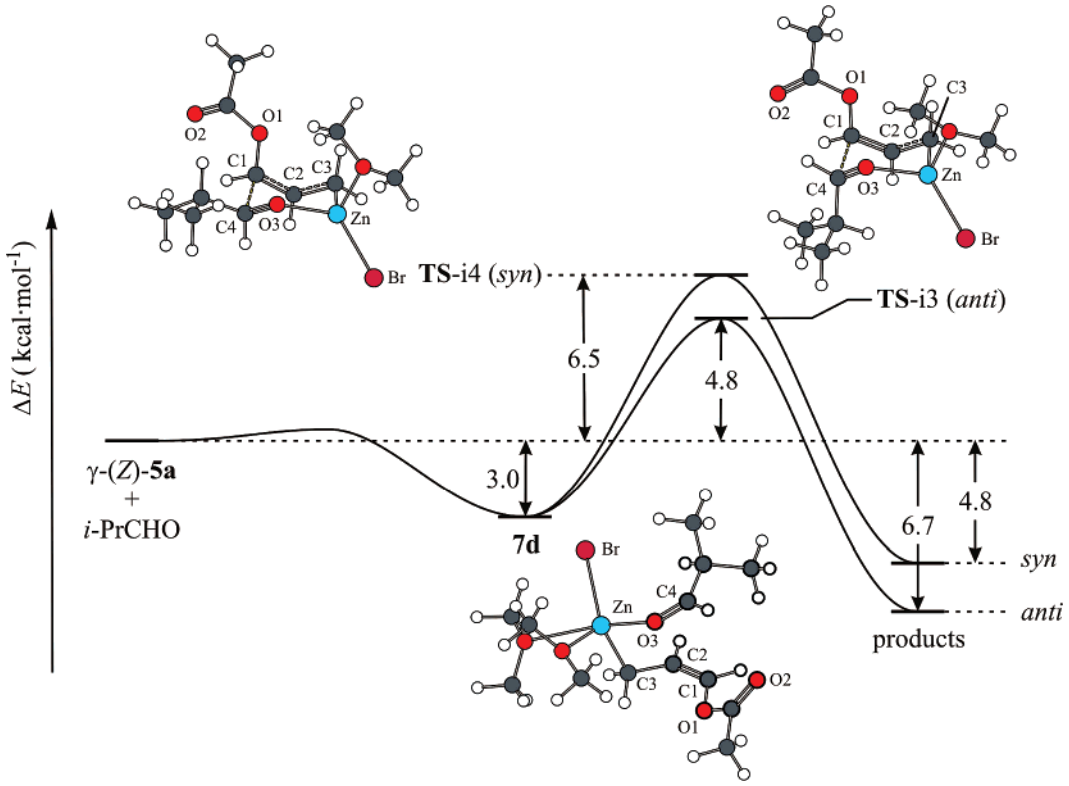

FIGURE 5. Energy profile for the addition of γ-(*Z*)-**5a** to 2-methylpropanal (**1b**) obtained at the DFT level.

and of γ-(*Z*)-**5a** isomers to 2-methylpropanal (**1b**). Again, for each aldehyde/γ-zinc complex pair, two different diastereomeric reaction channels (leading to the *syn* or *anti* adducts, respectively) have been considered.

Addition of γ-(*E*)-5a Complex. The energy profile obtained for the γ-(*E*)-**5a** isomer is schematically represented in Figure 4. Selected bond lengths for the intermediate **7c** and the two transition structures **TS-i1** and **TS-i2** are collected in Table 6.

As previously observed, the first reaction step is the formation of the preliminary complex between aldehyde and the metal, which adopts a penta-coordination (**7c**). This leads to a stabilization of 2.5 kcal mol^{-1}. As found before, this region of the potential surface is extremely flat and no transition state for the formation of **7c** exists. In the subsequent step, the *re* faces of the two reagents (*re*−*re* approach) or, alternatively, the *re* and *si* faces (*re*−*si* approach) can be involved in the attack. The *syn* and *anti* products are obtained in the former and latter cases, respectively. A chair-like six-membered transition state (**TS-i2**, leading to the *syn* product) has been located for the *re*−*re* approach, with an intrinsic energy barrier of 8.6 kcal mol^{-1}. In **TS-i2**, the C1−C2 and C2−C3 distances have values intermediate between single and double bonds (1.390 and 1.417 Å, respectively), while the newly forming C1−C4 bond is 2.180 Å. **TS-i1** is the most stable transition state located for the *re*−*si* approach. This chair-like structure corresponds to an energy barrier of 7.9 kcal mol^{-1}. Here, the isopropyl and acetate substituents have a 1,2-*trans*-diaxial orientation, and the dimethylether coordinated to the metal has a pseudo-equatorial position. The C1−C2 and C2−C3 bond distances are 1.388 and 1.420 Å, respectively, while the two carbon atoms forming the new C1−C4 bond are 2.205 Å far away. Thus, the calculations indicate a slight preference for **TS-i1**, leading to the *anti* product, the total energy difference ($\Delta\Delta E^{\ddagger}$) being 0.7 kcal mol^{-1}. The corresponding free energy difference ($\Delta\Delta G^{\ddagger}$) becomes 1.4 kcal mol^{-1}. This $\Delta\Delta G^{\ddagger}$ value would afford a diastereoselectivity above 80%, in fairly good agreement with the experiment.

TABLE 7. Selected Bond Lengths (Å) for 7d, TS-i3, and TS-i4

	Zn−Br	Zn−O3	Zn−C3	C1−C2	C2−C3	C1−C4
7d	2.405	2.433	2.022	1.340	1.481	3.719
TS-i3	2.373	2.007	2.133	1.385	1.418	2.211
TS-i4	2.365	2.004	2.133	1.388	1.416	2.238

Addition of γ-(*Z*)-5a Complex. The energy profile computed for the γ-(*Z*)-**5a** isomer is reported in Figure 5. Selected bond lengths for the intermediate **7d** and the following transition states (**TS-i3** and **TS-i4**) are given in Table 7.

The formation of the preliminary intermediate (**7d**, 3.0 kcal mol^{-1} below reactants), where the aldehyde is coordinated to the metal, again does not require any activation barrier. The intrinsic activation barriers for **TS-i3** and **TS-i4** are 7.8 and 9.5 kcal mol^{-1}, respectively. Thus, the energy difference between the two transition states (1.7 kcal mol^{-1}) is larger than that found for γ-(*E*)-**5a**. The corresponding Gibbs free energy difference ($\Delta\Delta G^{\ddagger}$) is 1.5 kcal mol^{-1}, thus confirming the diastereopreference for the formation of the *anti* isomer.

To obtain a complete description also for the reactions involving 2-methylpropanal, we have carried out MP2 computations with full geometry optimization on **TS-i1**, **TS-i2**, **TS-i3**, and **TS-i4** and the corresponding intermediates **7c** and **7d**. At the MP2 level, **TS-i1** and **TS-i2** become closer in energy (the corresponding energy barriers are 14.9 and 14.7 kcal mol^{-1}, respectively), while the energy gap between **TS-i3** and **TS-i4** increases (from 1.7 to 3.1 kcal mol^{-1}). In this case, the corresponding energy barriers are 14.8 and 17.9 kcal mol^{-1} and confirm the preference for the formation of the *anti* isomer.

Finally, it is worthy to comment shortly on the effect of the MP2 optimization on the structural features of the various critical

points. The MP2 geometrical parameters of the transition states are, in general, very similar to those obtained at the DFT level. The only significant difference has been found in the C1−C4 distance (C1 and C4 are the two atoms involved in the formation of the new bond). This parameter is slightly longer at the MP2 level, the difference with respect to DFT ranging from 0.05 Å in **TS-i1** to 0.14 Å in **TS-b2**. The other critical points do not show any remarkable difference when we compared the two computational levels.

Conclusions

In the present paper, we report the results of a combined experimental and theoretical study on the reaction of 3-bromopropenyl acetate in the presence of zinc with three different aldehydes [i.e., benzaldehyde (**1a**), 2-methylpropanal (**1b**), and cyclohexane carboxaldehyde (**1c**)]. With both saturated aldehydes, a 80% de in favor of the *anti* product is obtained, while for benzaldehyde, a 1:1 *syn*/*anti* ratio is observed. The structure and energy of the three possible η^1-allylic organozinc complexes (deriving from the insertion of a zinc atom into the carbon−bromine bond of 3-bromopropenyl acetate) have been investigated at the DFT computational level. The fluxional equilibrium between the three species involves two η^3 transition states (**TS-1** and **TS-2**). The computed activation barriers indicate a significant configurational stability of the η^1-allylic organozinc species at room temperature. This stability is probably due to the presence of the acetoxy substituent on the allylic terminus since, on the contrary, simple diallyl zinc complexes are known to behave as rapidly equilibrating species on the NMR time scale.[14]

The subsequent reaction step has been modeled using either benzaldehyde or 2-methylpropanal. In both cases, two competitive reaction paths leading to the *syn* and *anti* adducts originate from each γ-**5a** isomer. The energy and structure of the corresponding transition states have been compared. The computations show an apparent *anti* preference for the reaction of 2-methylpropanal with both γ-(*Z*)-**5a** and γ-(*E*)-**5a** (a diastereomeric excess larger than 80% is predicted considering the Gibbs free energy). Conversely, while the reaction of γ-(*Z*)-**5a** with benzaldehyde retains an *anti* stereopreference (de of about 70%), that involving γ-(*E*)-**5a** is characterized by two transition states with identical energy.

These computational results are in good agreement with the experimental observations in the case of 2-methylpropanal, a remarkable *anti* stereopreference being predicted on a theoretical basis, irrespective of the geometry of the starting allylic organometallic species. The lower energy calculated for **TS-i3** with respect to **TS-i4** (and also for **TS-b3** with respect to **TS-b4**) warns also against a noncritical application of the Zimmermann−Traxler model, which generally anticipates a *syn*-selectivity when a *Z*-configured allylic organometallic compound or a *Z*-enolate adds to an aldehyde through a pericyclic TS.

The agreement between computations and experiments in the case of benzaldehyde would be satisfactory under the assumption that the initial oxidative addition affords the γ-(*E*)-**5a** zinc complex only (where the two subsequent transition states, **TS-b1** and **TS-b2**, are at the same energy), irrespective of the starting isomeric ratio of 3-bromopropenyl acetate **4a**. This would mean that the way to oxidative addition affording γ-(*E*)-**5a** has lower activation energy than that leading to γ-(*Z*)-**5a**. Validation of this hypothesis would need, of course, an additional theoretical investigation concerning the insertion process of the zinc atom into the C−Br bond in **4a**.[15]

Also, it is important to stress that an exhaustive rationalization of the experimental evidence requires that, in our model, the formation of γ-(*E*)-**5a** and/or γ-(*Z*)-**5a** is favored with respect to that of α-**5a** which would afford the non-observed product (i.e., the 4-hydroxyenol acetate derivatives). For sake of completeness, the reaction profile of aldehydes with α-**5a** has been computed. The results are described in detail in the Supporting Information. These data show that the activation barriers that characterize this reaction profile are similar to those found for γ-(*E*)-**5a** and γ-(*Z*)-**5a**.

Our computations have shown that **TS-b4** (Figure 3) and **TS-b1** (Figure 2), leading to the *syn* adduct and the *anti* adduct, respectively, have interesting structural features: the phenyl ring and the acetate group are placed on almost parallel planes, a relative orientation which favors stabilizing π-stacking interactions. To evaluate the importance of these interactions, we have carried out MP2 computations on all transitions states and intermediates with full geometry optimization. The results obtained for **TS-b1**, **TS-b2**, **TS-b3**, and **TS-b4** are particularly interesting and confirm the importance of π-stacking effects. In particular, at the MP2 level, while **TS-b1** and **TS-b2** are still very close in energy, the energy difference between **TS-b4** and **TS-b3** decreases. This computational result indicates that the effect of π-stacking interactions is that of making **TS-b4** and **TS-b3** closer in energy, and consequently, the diastereoselectivity in favor of the *anti* product (as obtained at the DFT level) is predicted to decrease, in agreement with the experimental evidence.

Acknowledgment. This work was supported by MIUR (Rome) PRIN project grant "Sintesi e Stereocontrollo di Molecole Organiche per lo Sviluppo di Metodologie Innovative di Interesse Applicativo".

Supporting Information Available: Detailed experimental procedures and characterizations for **4a**−**c** and **6a**−**c**; Cartesian coordinates and detailed figures for all of the various critical points located on the potential surface. This material is available free of charge via the Internet at http://pubs.acs.org.

JO701661Z

(14) Guijarro, A. In *The Chemistry of Organozinc Compounds, Part 1*; Rappoport, Z., Marek, I., Eds.; Wiley: Chichester, UK, 2006; Chapter 6.

(15) A detailed NMR study on penta-2,4-dienyl zinc chloride complexed with TMEDA revealed that only the *E* isomer is detectable in solution and in the solid state: Yasuda, H.; Ohnuma, A.; Nakamura, A.; Kai, Y.; Yasuoka, N.; Kasai, N. *Bull. Chem. Soc. Jpn.* **1980**, *53*, 1089.